Element-wise and recursive solutions for the power spectral density of biological stochastic dynamical systems at fixed points

Shivang Rawat [1,2,*] and Stefano Martiniani [1,2,3,†]

[1] *Courant Institute of Mathematical Sciences, New York University, New York 10003, USA*
[2] *Center for Soft Matter Research, Department of Physics, New York University, New York 10003, USA*
[3] *Simons Center for Computational Physical Chemistry, Department of Chemistry, New York University, New York 10003, USA*

(Received 26 December 2023; accepted 6 September 2024; published 20 November 2024)

Stochasticity plays a central role in nearly every biological process, and the noise power spectral density (PSD) is a critical tool for understanding variability and information processing in living systems. In steady state, many such processes can be described by stochastic linear time-invariant (LTI) systems driven by Gaussian white noise, whose PSD is a complex rational function of the frequency that can be concisely expressed in terms of their Jacobian, dispersion, and diffusion matrices, fully defining the statistical properties of the system's dynamics at steady state. Here, we arrive at compact, element-wise solutions of the rational function coefficients for the auto- and cross-spectrum that enable the explicit analytical computation of the PSD in dimensions $n = 2, 3, 4$. We further present a recursive Leverrier-Faddeev-type algorithm for the exact computation of the rational function coefficients. Crucially, both solutions are free of matrix inverses. We illustrate our element-wise and recursive solutions by considering the stochastic dynamics of neural systems models, namely, FitzHugh-Nagumo ($n = 2$), Hindmarsh-Rose ($n = 3$), Wilson-Cowan ($n = 4$), and the stabilized supralinear network ($n = 22$), as well as an evolutionary game-theoretic model with mutations ($n = 5, 31$). We extend our approach to derive a recursive method for calculating the coefficients in the power-series expansion of the integrated covariance matrix for interacting spiking neurons modeled as Hawkes processes on arbitrary directed graphs.

DOI: 10.1103/PhysRevResearch.6.043179

Unlike in an abstract painting by Mondrian [1], the world is not made of perfect forms. Rather, we are surrounded by imperfect, yet regular patterns emerging from the randomness of microscopic processes that collectively give rise to statistically predictable phenomena. A point in case is the derivation of the diffusion equation from the random (Brownian) motion of microscopic particles [2,3]. This is but one example of the many processes that can be recapitulated in terms of ordinary differential equations driven by random processes, known as stochastic differential equations (SDEs). For instance, the effect of thermal fluctuations on synaptic conductance (linked to the stochastic opening of voltage-gated ion channels) and on the voltage of an electrical circuit (Johnson's noise), or the fluctuations of a neuron's membrane potential driven by stochastic spike arrival, can all be modeled as SDEs. Alternatively, SDEs are commonly adopted to model processes for which the exact dynamics are not known, and it is thus appropriate to express the model in terms of random variables encoding our uncertainty about the state of the system. Examples are the trajectory of an aircraft as modeled by navigation systems, or the evolution of stock prices subject to market fluctuations [4].

Among stochastic models, linear time-invariant (LTI) SDEs play a special role because (i) they are amenable to analytical treatment and (ii) the linear response of many nonlinear systems (e.g., around a fixed point of the dynamics) can be reduced to LTI SDEs. To make this point explicit, let us consider a nonlinear autonomous dynamical system driven by additive white noise with finite variance, namely,

$$\mathrm{d}\mathbf{x} = \mathbf{f}(\mathbf{x})\mathrm{d}t + \mathbf{L}\mathrm{d}\mathbf{W}, \tag{1}$$

where $\mathbf{x} \in \mathbb{R}^n$ is the state vector, $\mathbf{f} : \mathbb{R}^n \to \mathbb{R}^n$ is a nonlinear drift function encoding the deterministic dynamics, $\mathbf{L} \in \mathbb{R}^{n\times m}$ is the *dispersion* matrix defining how noise enters the system, and $\mathrm{d}\mathbf{W} \in \mathbb{R}^m$ is a vector of mutually independent Gaussian increments satisfying $\mathbb{E}[\mathrm{d}\mathbf{W}\mathrm{d}\mathbf{W}^\top] = \mathbf{D}\mathrm{d}t$, where $\mathbf{D}$ is the *diffusion* matrix (or spectral density matrix) with entries $D_{ij} = \delta_{ij}\sigma_i^2$, where δ_{ij} is the Kronecker delta [4].

We are interested in the power spectral density (PSD) of the system's response, $\mathbf{x}(t)$, near a stable fixed point, $\mathbf{x}_0$, so we proceed by linearizing the drift function about this point, yielding the following LTI system:

$$\mathrm{d}\mathbf{x} = \mathbf{J}\mathbf{x}\mathrm{d}t + \mathbf{L}\mathrm{d}\mathbf{W}, \tag{2}$$

where we have redefined $\mathbf{x}(t) \equiv \mathbf{x}(t) - \mathbf{x}_0$ such that $\mathbf{x}(t_0) = \mathbf{0}$, and $\mathbf{J} = |\mathrm{d}\mathbf{f}/\mathrm{d}\mathbf{x}|_{\mathbf{x}_0} \in \mathbb{R}^{n\times n}$ is the Jacobian evaluated at the fixed point, that we take to be Hurwitz (real part of all eigenvalues less than zero) to assure stability. The solution to this linear SDE is given by the stochastic integral

*Contact author: sr6364@nyu.edu
†Contact author: sm7683@nyu.edu

$\mathbf{x}(t) = \int_{-\infty}^{t} e^{\mathbf{J}(t-s)}\mathbf{L}d\mathbf{W}(s)$, which is a zero-mean stationary process with covariance $\mathcal{R}(\tau)$.

The PSD of this stochastic process is known to be expressed in terms of the following matrix product (see [5] and Supplemental Material [6]):

$$\mathcal{S}_{\mathbf{x}}(\omega) = (i\omega\mathbf{I} + \mathbf{J})^{-1}\,\mathbf{L}\,\mathbf{D}\,\mathbf{L}^{\top}(-i\omega\mathbf{I} + \mathbf{J})^{-\top}. \tag{3}$$

For the sake of brevity, from now on we refer to $\mathcal{S}_{\mathbf{x}}(\omega)$ as $\mathcal{S}(\omega)$, whose i, jth entry is denoted $\mathcal{S}^{ij}(\omega)$. $\mathcal{S}(\omega)$ is a product of the spectral factors (the transfer function matrix) of the dynamical system and can be expressed as a rational function of the following form (see [7,8] and Appendix A):

$$\begin{aligned}\mathcal{S}(\omega) &= \frac{\mathbf{P}(\omega) + i\omega\mathbf{P}'(\omega)}{Q(\omega)} \\ &= \frac{\sum_{\alpha=0}^{n-1}\mathbf{P}_\alpha\omega^{2\alpha} + i\omega\sum_{\alpha=0}^{n-2}\mathbf{P}'_\alpha\omega^{2\alpha}}{\sum_{\alpha=0}^{n} q_\alpha\omega^{2\alpha}},\end{aligned} \tag{4}$$

and the corresponding PSD matrix elements are of the form

$$\mathcal{S}^{ij}(\omega) = \frac{P^{ij}(\omega) + i\delta_{ij}\omega P^{ij\prime}(\omega)}{Q(\omega)}, \tag{5}$$

where $P^{ij}(\omega) = \sum_{\alpha=0}^{n-1} p_\alpha^{ij}\omega^{2\alpha}$, $P^{ij\prime}(\omega) = \sum_{\alpha=0}^{n-2} p_\alpha^{ij\prime}\omega^{2\alpha}$, and $Q(\omega) = \sum_{\alpha=0}^{n} q_\alpha\omega^{2\alpha}$ are even-powered polynomials with real coefficients (p_α^{ij}, $p_\alpha^{ij\prime}$, and q_α).

In this work we derive closed-form expressions for the individual coefficients of the rational function of a given element of $\mathcal{S}(\omega)$, i.e., $\mathcal{S}^{ij}(\omega)$. In Sec. II we provide the formulas for the autospectrum of two-, three-, and four-dimensional (2D, 3D, 4D) systems expressed in terms of elementary trace operations applied to the submatrices of $\mathbf{J}$. The element-wise solutions for the auto- and cross-spectrum of a generic n-dimensional system are presented in the Supplemental Material [6], and they can be obtained directly in symbolic form through our software (see Sec. V).

In Sec. III we derive a recursive algorithm (Theorem 1) to calculate the coefficient matrices $\mathbf{P}_\alpha$ and $\mathbf{P}'_\alpha$ and the coefficients of the denominator, q_α. We follow an approach similar to the one adopted by Hou [9] to derive the Leverrier-Faddeev (LF) method, which is a recursive approach to find the characteristic polynomial of a matrix in $O(n^4)$ operations, where n is the dimensionality of the system [10,11]. Note that unlike Eq. (3), our solutions are free of matrix inverses, which is numerically advantageous when the system is ill conditioned. To demonstrate the wide applicability of the recursive algorithm, we derive a recursive solution for the rational function of an auxiliary spectral matrix, Appendix B. Using this solution we develop a recursive method (Theorem 2) to find the power-series expansion of the integrated covariance matrix of the Hawkes process [12] with arbitrary connectivity (Sec. IV).

In Sec. IV we apply our solutions to several stochastic nonlinear models from neuroscience and evolutionary biology, providing model-specific solutions for the auto-spectrum when appropriate. In practice, readers seeking analytical expressions for the auto-spectrum of specific models (e.g., FitzHugh-Nagumo [13–15], or Hindmarsh-Rose [16]) can refer directly to Secs. I and IV.

I. PRELIMINARY EXAMPLES

Before presenting the general solutions, it is instructive to review concrete one- and two-dimensional cases that are commonly encountered in the literature, for which we can derive the coefficients analytically with little effort, without resorting to our sophisticated solutions. To this end, let us consider the simplest and most common case: the auto-spectrum of an LTI system with mutually independent additive noise (i.e., $\mathbf{L} = \mathbf{I}$). For the $d = 1$ case, also known as the Ornstein-Uhlenbeck process, we have

$$\mathrm{d}x = -\tau_r^{-1}x\mathrm{d}t + \mathrm{d}W \tag{6}$$

with $\mathrm{d}W^2 = \sigma^2\mathrm{d}t$. It can be seen from Eq. (3) that

$$\mathcal{S}(\omega) = \frac{\sigma^2}{\tau_r^{-2} + \omega^2}, \tag{7}$$

so that the coefficients in Eq. (5) are $p_0^{11} = \sigma^2$, $q_0 = \tau_r^{-2}$, and $q_1 = 1$ [17].

A slightly more sophisticated example is the stochastic FitzHugh-Nagumo model [13–15], which amounts to a simplification of the Hodgkin-Huxley equations for action potential generation [18]. We simulate the dynamical evolution of a neuron's membrane potential in response to an input current by the following set of SDEs:

$$\begin{aligned}\frac{\mathrm{d}v}{\mathrm{d}t} &= \left(v - \frac{v^3}{3} - w + I\right) + h_1(v)\eta_1 \\ \frac{\mathrm{d}w}{\mathrm{d}t} &= \epsilon(v + \alpha - \beta w) + h_2(w)\eta_2.\end{aligned} \tag{8}$$

Here, v represents the difference between the membrane potential and the resting potential, w is the variable associated with the recovery of the ion channels after the generation of an action potential, and I is the external current input. The parameters α and β are related to the activation threshold of the fast sodium channel and the inactivation threshold of the slow potassium channels, respectively. $\epsilon \ll 1$ sets the timescale for the evolution of the activity, making the dynamics of v much faster than those of w. In the subthreshold regime, the fixed point, (v_e, w_e), can be found analytically as a function of the parameters of the model and the input current (details in Supplemental Material [6]). The stochasticity in v and w is represented by two uncorrelated Gaussian white noise sources, η_1 and η_2, with a standard deviation of 1. We consider the case of multiplicative noise which is realized by setting $h_1(v)$ and $h_2(w)$ proportional to the respective function variables. Specifically, we set $h_1(v) = 0$ and $h_2(w) = \sigma w$. We choose the variance of the noise small enough that we are always in the vicinity of the fixed point. Then, upon linearizing Eq. (8) around the fixed point, (v_e, w_e), we arrive at the following LTI SDEs:

$$\begin{bmatrix}\dot{v}\\ \dot{w}\end{bmatrix} = \begin{bmatrix}1 - v_e^2 & -1\\ \epsilon & -\beta\epsilon\end{bmatrix}\begin{bmatrix}v - v_e\\ w - w_e\end{bmatrix} + \sigma\begin{bmatrix}0 & 0\\ 0 & w_e\end{bmatrix}\begin{bmatrix}\eta_1\\ \eta_2\end{bmatrix}. \tag{9}$$

Plugging the Jacobian and noise matrices into Eq. (3), we obtain the PSD of the membrane potential, v, as

$$\begin{aligned}\mathcal{S}_v(\omega) = w_e^2\sigma^2 / \big[&\big[\epsilon + \big(v_e^2 - 1\big)\beta\epsilon\big]^2 \\ &+ \big[\big(v_e^2 - 1\big)^2 - 2\epsilon + \beta^2\epsilon^2\big]\omega^2 + \omega^4\big],\end{aligned} \tag{10}$$

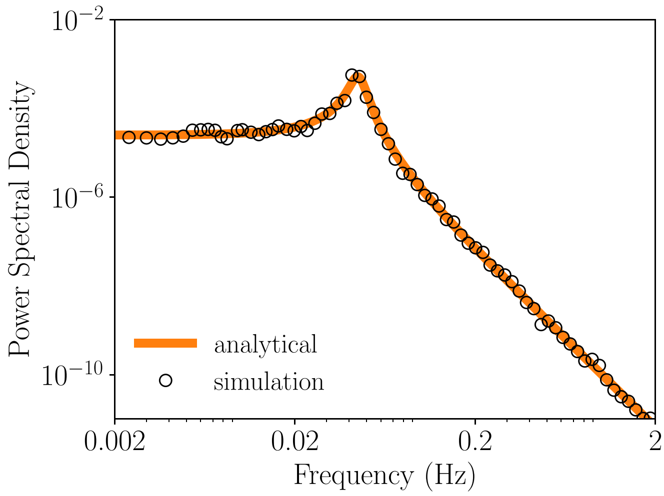

FIG. 1. Power spectral density of the membrane potential for the FitzHugh-Nagumo model. A comparison of the PSD of the membrane potential (v) calculated via simulation and the analytical rational function solution. The parameters used to simulate the system are $I = 0.265$, $\alpha = 0.7$, $\beta = 0.75$, and $\epsilon = 0.08$, which yields a fixed-point solution $v_e = -1.001\,25$, $w_e = -0.401\,665$. Here, we plot the auto-spectrum for the case of multiplicative noise, i.e., $h_1(v) = 0$ and $h_2(w) = \sigma w$, where $\sigma = 0.001$.

so that in Eq. (5) we have $p_0^{11} = w_e^2\sigma^2$, $p_1^{11} = 0$, $q_0 = [\epsilon + (v_e^2 - 1)\beta\epsilon]^2$, $q_1 = [(v_e^2 - 1)^2 - 2\epsilon + \beta^2\epsilon^2]$, and $q_2 = 1$. We verify the accuracy of this solution, Eq. (10), by comparison with the PSD obtained numerically by simulating the nonlinear model, Eq. (8), with multiplicative noise, and find excellent agreement as shown in Fig. 1.

This laborious approach works well for systems with dimensions $n = 1, 2$, but it becomes infeasible in higher dimensions. This is due to the multiplication of inverses of two matrices with complex entries, $(i\omega\mathbf{I} + \mathbf{J})^{-1}$ and $(-i\omega\mathbf{I} + \mathbf{J})^{-\top}$.

II. ELEMENT-WISE SOLUTION

We now introduce element-wise solutions for the auto-spectrum of two-, three-, and four-dimensional systems. The general n-dimensional solutions for both auto- and cross-spectrum can be found in the Supplemental Material [6] alongside their derivations and can be conveniently obtained in symbolic form for any dynamical system through our software (see Sec. V). This method relies on expressing the rational function expression of Eq. (3) in terms of elementary matrix operations on submatrices of the Jacobian, $\mathbf{J}$. Although this approach requires roughly $O(n^4 \log n)$ (Supplemental Material [6], Fig. S2), operations for each element of the PSD matrix, i.e., $O(n^6 \log n)$ total, it is particularly valuable to arrive at analytical closed-form solutions for the auto- or cross-spectra of specific dynamical variables, yielding greater insight into the dependence of the power spectral density on the model's functional form and its parameters. For simplicity, we consider the auto-spectrum of an LTI system driven by uncorrelated white noise (see Supplemental Material [6] for the most general case of correlated noise and/or the cross-spectrum).

We start by noting that the denominator in Eq. (5) is independent of the type of noise driving the system, and it can be written as an even-powered expansion in ω with real coefficients. Similarly, the numerator of the auto-spectrum is an even-powered expansion in ω with real coefficients, but they depend directly on how the noise is added via the dispersion matrix, $\mathbf{L}$, whose elements we denote l_{ij}. For the particular case of independent noise, i.e., $l_{ij} = 0$ for $i \neq j$, the coefficient of $\omega^{2\alpha}$ in the numerator of the rational function for the ith variable takes the simplified form

$$p_\alpha^{ii} = \sigma_i^2\, l_i^2\, d^\alpha(\mathbf{O}_{ii}) + \sum_{\substack{j=1\\ j\neq i}}^{n} \sigma_j^2\, l_j^2\, f^\alpha(\mathbf{O}_{ji}, \mathbf{e}_{\min(i,j)}), \tag{11}$$

where $d^\alpha(\mathbf{O}_{ii})$ and $f^\alpha(\mathbf{O}_{ji})$ are functions of the Jacobian submatrices, $\mathbf{O}_{ij}$, defined according to the algorithm in Fig. 2. The functions themselves can be expressed in terms of Bell polynomials [19] and are defined in the Supplemental Material [6] (Sec. 5). $\mathbf{e}_\beta \in \{0, 1\}^{n-1\times 1}$ is the standard unit vector equal to 1 at index $\beta = \min(i, j)$ and 0 everywhere else. $\sigma_i^2 \equiv \sigma_{ii}^2$ is the ith diagonal entry of the noise matrix $\mathbf{D}$, and, since $\mathbf{L}$ is diagonal, we also use the notation $l_i \equiv l_{ii}$.

Here, we only provide the solution for the auto-spectrum of the first variable, i.e., $i = 1$. This solution can be generalized for any variable $i \neq 1$, as shown in the Supplemental Material [6]. Alternatively, one can simply interchange the rows and columns of the LTI system so that the variable of interest appears at index $i = 1$ and directly use the solution reported in this section.

Since the coefficients of the denominator are the same for all dimensions, n, we define them first,

$$\begin{aligned}
q_{n-4} &= \frac{1}{24}[\mathrm{Tr}^4(\mathbf{J}^2) - 6\mathrm{Tr}^2(\mathbf{J}^2)\mathrm{Tr}(\mathbf{J}^4)\\
&\quad + 8\mathrm{Tr}(\mathbf{J}^2)\mathrm{Tr}(\mathbf{J}^6) + 3\mathrm{Tr}^2(\mathbf{J}^4) - 6\mathrm{Tr}(\mathbf{J}^8)]\\
q_{n-3} &= \frac{\mathrm{Tr}^3(\mathbf{J}^2) - 3\mathrm{Tr}(\mathbf{J}^2)\mathrm{Tr}(\mathbf{J}^4) + 2\mathrm{Tr}(\mathbf{J}^6)}{6}\\
q_{n-2} &= \frac{\mathrm{Tr}^2(\mathbf{J}^2) - \mathrm{Tr}(\mathbf{J}^4)}{2}\\
q_{n-1} &= \mathrm{Tr}(\mathbf{J}^2)\\
q_n &= 1.
\end{aligned} \tag{12}$$

Note that for each n we will only need to consider the coefficients q_α with $\alpha \geqslant 0$.

A. 2D solution

For a 2D system, we can write the auto-spectrum of the first variable as

$$\mathcal{S}^{11}(\omega) = \frac{p_0 + p_1\omega^2}{q_0 + q_1\omega^2 + q_2\omega^4}, \tag{13}$$

where the coefficients of the numerator are given by the equations

$$\begin{aligned}
p_0 &= l_1^2\sigma_1^2\mathrm{Tr}(\mathbf{O}_{11}^2) + l_2^2\sigma_2^2\mathrm{Tr}(\mathbf{O}_{21}^2),\\
p_1 &= l_1^2\sigma_1^2.
\end{aligned} \tag{14}$$

Here, the matrices $\mathbf{O}_{11} = [a_{22}]$ and $\mathbf{O}_{21} = [a_{12}]$ are found from the 2D Jacobian using the algorithm summarized in

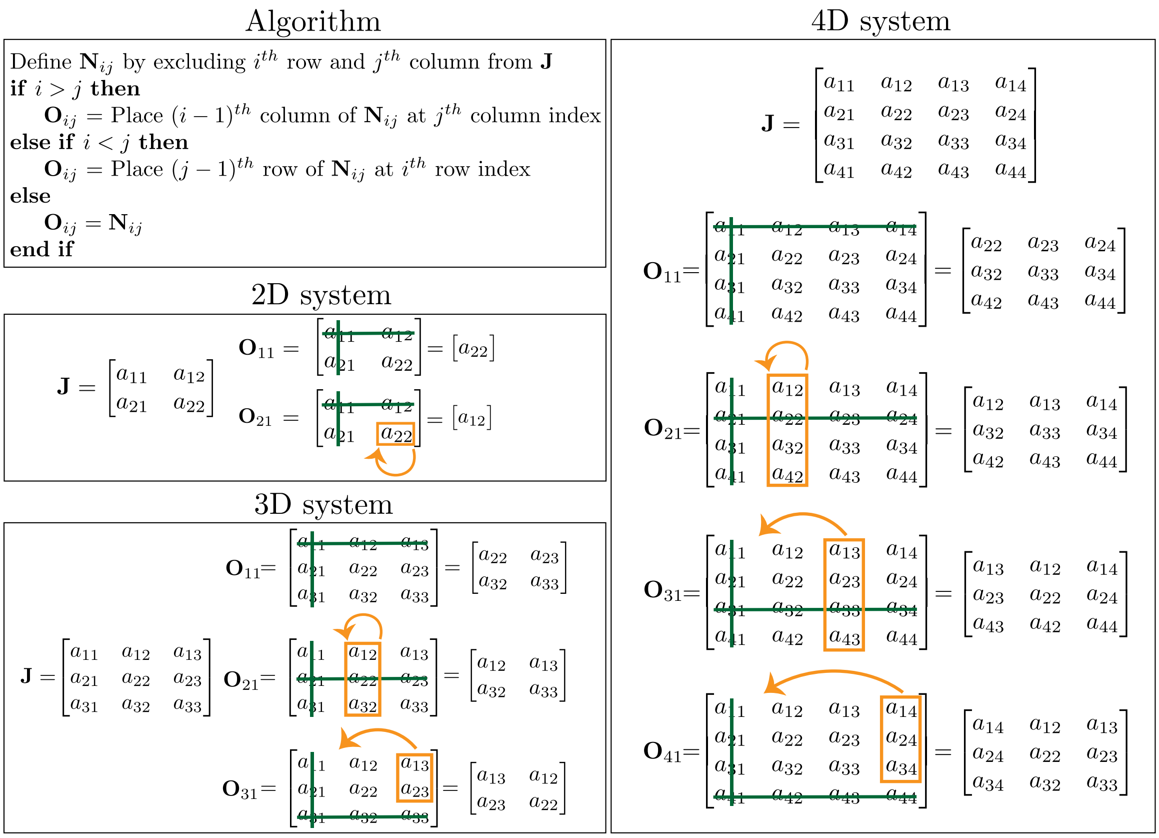

FIG. 2. Definitions of $\mathbf{O}_{ij}$ matrices. We show the algorithm to generate the $\mathbf{O}_{ij}$ matrices with examples for the 2D, 3D, and 4D systems. To find $\mathbf{O}_{ij}$, we have to first find the excluded matrix by removing the ith row and jth column (denoted by green lines) from the Jacobian matrix and then perform the row/column change operations, denoted by orange arrows.

Fig. 2 (*n.b.*, we denote a_{ij} the i, jth entry of the Jacobian). The coefficients of the denominator are given by the last three entries of Eq. (12).

B. 3D solution

For a 3D system, the auto-spectrum of the first variable takes the form

$$\mathcal{S}^{11}(\omega) = \frac{p_0 + p_1\omega^2 + p_2\omega^4}{q_0 + q_1\omega^2 + q_2\omega^4 + q_3\omega^6}, \tag{15}$$

where the coefficients of the numerator are given by the equations

$$\begin{aligned} p_0 &= \frac{1}{2}\Bigg[l_1^2\sigma_1^2\big(\mathrm{Tr}^2\big(\mathbf{O}_{11}^2\big) - \mathrm{Tr}\big(\mathbf{O}_{11}^4\big)\big) + \sum_{j=2}^{3} l_j^2\sigma_j^2\big(\mathrm{Tr}^2\big({\mathbf{O}'_{j1}}^2\big) \\ &\quad - \mathrm{Tr}\big({\mathbf{O}'_{j1}}^4\big) + \mathrm{Tr}^2\big(\mathbf{O}_{j1}^2\big) - \mathrm{Tr}\big(\mathbf{O}_{j1}^4\big)\big)\Bigg] \\ p_1 &= l_1^2\sigma_1^2\mathrm{Tr}\big(\mathbf{O}_{11}^2\big) + \sum_{j=2}^{3} l_j^2\sigma_j^2\big(-2\mathrm{Tr}(\mathbf{O}'_{j1})\mathrm{Tr}(\mathbf{O}_{j1}) \\ &\quad + \mathrm{Tr}\big({\mathbf{O}'_{j1}}^2\big) + \mathrm{Tr}^2(\mathbf{O}_{j1})\big) \\ p_2 &= l_1^2\sigma_1^2. \end{aligned} \tag{16}$$

Here, the matrices $\mathbf{O}_{11}$, $\mathbf{O}_{21}$, and $\mathbf{O}_{31}$ are found from the 3D Jacobian matrix using the algorithm summarized in Fig. 2. Furthermore, the matrices $\mathbf{O}'_{ij}$ are found by excluding the kth row and column from the corresponding $\mathbf{O}_{ij}$ matrix, where $k = \min(i, j)$. Since we are interested in the spectrum of the first variable ($j = 1$), $k = \min(i, 1) = 1$. Thus, $\mathbf{O}'_{21}$ and $\mathbf{O}'_{31}$ are found by removing the first row and column from the matrices $\mathbf{O}_{21}$ and $\mathbf{O}_{31}$, respectively. The coefficients of the denominator are given by the last four entries of Eq. (12).

If the variance of the noise is the same for all the variables, i.e., $l_1^2\sigma_1^2 = l_2^2\sigma_2^2 = l_3^2\sigma_3^2 = \sigma^2$, we can further simplify the coefficients of the numerator, which become

$$\begin{aligned} p_0 &= \sigma^2\det(\mathbf{A}^\top\mathbf{A}) \\ p_1 &= \sigma^2\mathrm{Tr}\big(\mathbf{A}_1^\top\mathbf{A}_1 + \mathbf{A}_2^2\big) \\ p_2 &= \sigma^2, \end{aligned} \tag{17}$$

where $\mathbf{A} \in \mathbb{R}^{3\times 2}$ is the submatrix of $\mathbf{J}$ obtained by removing its first column. Then, $\mathbf{A}_1 \in \mathbb{R}^{1\times 2}$ is the submatrix obtained by isolating the first row of $\mathbf{A}$, and $\mathbf{A}_2 \in \mathbb{R}^{2\times 2}$ is the submatrix obtained by removing the first row of $\mathbf{A}$.

C. 4D solution

For a 4D system, the auto-spectrum of the first variable becomes

$$\mathcal{S}^{11}(\omega) = \frac{p_0 + p_1\omega^2 + p_2\omega^4 + p_3\omega^6}{q_0 + q_1\omega^2 + q_2\omega^4 + q_3\omega^6 + q_4\omega^8}, \tag{18}$$

where the coefficients of the numerator are given by Eq. (19). Here, the matrices $\mathbf{O}_{11}$, $\mathbf{O}_{21}$, $\mathbf{O}_{31}$, and $\mathbf{O}_{41}$ are found from the

4D Jacobian matrix using the algorithm summarized in Fig. 2. Using an argument similar to the 3D case, $\mathbf{O}'_{21}$, $\mathbf{O}'_{31}$, and $\mathbf{O}'_{41}$ can be found by removing the first row and column from the matrices $\mathbf{O}_{21}$, $\mathbf{O}_{31}$, and $\mathbf{O}_{41}$, respectively. The coefficients of the denominator are given by Eq. (12):

$$\begin{aligned}
p_0 &= \frac{1}{6}\Bigg[l_1^2\sigma_1^2\big(\mathrm{Tr}^3\big(\mathbf{O}_{11}^2\big) - 3\mathrm{Tr}\big(\mathbf{O}_{11}^2\big)\mathrm{Tr}\big(\mathbf{O}_{11}^4\big) + 2\mathrm{Tr}\big(\mathbf{O}_{11}^6\big)\big) + \sum_{j=2}^{4} l_j^2\sigma_j^2\big(\mathrm{Tr}^3\big({\mathbf{O}'_{j1}}^2\big) - 3\mathrm{Tr}\big({\mathbf{O}'_{j1}}^2\big)\mathrm{Tr}\big({\mathbf{O}'_{j1}}^4\big) \\
&\quad + 2\mathrm{Tr}\big({\mathbf{O}'_{j1}}^6\big) + \mathrm{Tr}^3\big(\mathbf{O}_{j1}^2\big) - 3\mathrm{Tr}\big(\mathbf{O}_{j1}^2\big)\mathrm{Tr}\big(\mathbf{O}_{j1}^4\big) + 2\mathrm{Tr}\big(\mathbf{O}_{j1}^6\big)\big)\Bigg], \\
p_1 &= \frac{1}{6}\Bigg[3l_1^2\sigma_1^2\big(\mathrm{Tr}^2\big(\mathbf{O}_{11}^2\big) - \mathrm{Tr}\big(\mathbf{O}_{11}^4\big)\big) + \sum_{j=2}^{4} l_j^2\sigma_j^2\big(-3\big(\mathrm{Tr}^2\big(\mathbf{O}'_{j1}\big) - \mathrm{Tr}\big({\mathbf{O}'_{j1}}^2\big)\big)\big(\mathrm{Tr}^2(\mathbf{O}_{j1}) - \mathrm{Tr}\big(\mathbf{O}_{j1}^2\big)\big) + 3\mathrm{Tr}^2\big({\mathbf{O}'_{j1}}^2\big) \\
&\quad + 2\mathrm{Tr}\big(\mathbf{O}'_{j1}\big)\big(\mathrm{Tr}^3(\mathbf{O}_{j1}) - 3\mathrm{Tr}(\mathbf{O}_{j1})\mathrm{Tr}\big(\mathbf{O}_{j1}^2\big) + 2\mathrm{Tr}\big(\mathbf{O}_{j1}^3\big)\big) - 3\mathrm{Tr}\big({\mathbf{O}'_{j1}}^4\big) + 3\mathrm{Tr}^2\big(\mathbf{O}_{j1}^2\big) - 3\mathrm{Tr}\big(\mathbf{O}_{j1}^4\big)\big)\Bigg], \\
p_2 &= l_1^2\sigma_1^2\mathrm{Tr}\big(\mathbf{O}_{11}^2\big) + \sum_{j=2}^{4} l_j^2\sigma_j^2\big(\mathrm{Tr}^2\big(\mathbf{O}'_{j1}\big) + \mathrm{Tr}^2(\mathbf{O}_{j1}) - 2\mathrm{Tr}\big(\mathbf{O}'_{j1}\big)\mathrm{Tr}(\mathbf{O}_{j1})\big), \\
p_3 &= l_1^2\sigma_1^2.
\end{aligned} \tag{19}$$

III. RECURSIVE SOLUTIONS

We derive an alternative approach to computing the polynomial coefficients of the auto- and cross-spectrum based on a recursive algorithm. By this method we can obtain coefficients for all entries of the power spectral matrix simultaneously in $O(n^4)$ operations (Supplemental Material, Fig. S1). To make our solution compact, we denote the noise covariance matrix $\mathbf{C} \equiv \mathbf{L}\,\mathbf{D}\,\mathbf{L}^\top$. We specify the algorithm in the following theorem and provide a proof in Supplemental Material [6]. Note that the algorithm can alternatively be derived by leveraging the Barnett-Leverrier recursive formula [20].

Theorem 1. The noise power spectral density matrix of an LTI system is a complex-valued rational function of the form

$$\begin{aligned}
\mathcal{S}(\omega) &= (i\omega\mathbf{I} + \mathbf{J})^{-1}\,\mathbf{C}\,(-i\omega\mathbf{I} + \mathbf{J})^{-\top} \\
&= \frac{\sum_{\alpha=0}^{n-1}\mathbf{P}_\alpha\omega^{2\alpha} + i\omega\sum_{\alpha=0}^{n-2}\mathbf{P}'_\alpha\omega^{2\alpha}}{\sum_{\alpha=0}^{n} q_\alpha\omega^{2\alpha}}.
\end{aligned}$$

The numerator's matrix coefficients are given by the recursive equations,

$$\begin{aligned}
\mathbf{P}'_{\alpha-1} &= \mathbf{J}\mathbf{P}_\alpha - \mathbf{P}_\alpha\mathbf{J}^\top - \mathbf{J}\mathbf{P}'_\alpha\mathbf{J}^\top, \\
\mathbf{P}_{\alpha-1} &= q_\alpha\mathbf{C} + \mathbf{P}'_{\alpha-1}\mathbf{J}^\top - \mathbf{J}\mathbf{P}'_{\alpha-1} - \mathbf{J}\mathbf{P}_\alpha\mathbf{J}^\top,
\end{aligned} \tag{20}$$

for $\alpha \in \{1, \dots, n\}$, starting from $\alpha = n$ with $\mathbf{P}_n = \mathbf{P}'_n = \mathbf{0}$. The scalar coefficients of the denominator can be recursively calculated using

$$q_\alpha = \frac{1}{n-\alpha}[\mathrm{Tr}(\mathbf{J}\mathbf{Q}'_{\alpha-1}) + \mathrm{Tr}(\mathbf{J}\mathbf{Q}_\alpha\mathbf{J}^\top)], \tag{21}$$

if $\alpha < n$, and $q_n = 1$. The coefficients $\mathbf{Q}'_{\alpha-1}$ and $\mathbf{Q}_\alpha$ are given in turn by the recursive equations,

$$\begin{aligned}
\mathbf{Q}'_{\alpha-1} &= \mathbf{J}\mathbf{Q}_\alpha - \mathbf{Q}_\alpha\mathbf{J}^\top - \mathbf{J}\mathbf{Q}'_\alpha\mathbf{J}^\top, \\
\mathbf{Q}_{\alpha-1} &= q_\alpha\mathbf{I} + \mathbf{Q}'_{\alpha-1}\mathbf{J}^\top - \mathbf{J}\mathbf{Q}'_{\alpha-1} - \mathbf{J}\mathbf{Q}_\alpha\mathbf{J}^\top,
\end{aligned} \tag{22}$$

for $\alpha \in \{0, 1, \dots, n\}$, starting from $\alpha = n$ with $\mathbf{Q}_n = \mathbf{Q}'_n = \mathbf{0}$ and $\mathbf{Q}_{-1} = \mathbf{Q}'_{-1} = \mathbf{0}$.

Note that Eq. (22) is the same as Eq. (20) for $\mathbf{C} = \mathbf{I}$, and that the $\mathbf{P}'_\alpha$ ($\mathbf{Q}'_\alpha$) matrices are antisymmetric, whereas the $\mathbf{P}_\alpha$ ($\mathbf{Q}_\alpha$) matrices are symmetric.

The approach used to derive the recursive solution for $\mathcal{S}(\omega)$ is broadly applicable to matrices of similar forms. In Appendix B we provide an example of one such recursive algorithm for the similarly defined matrix,

$$\mathcal{T}(\omega) = (\omega\mathbf{I} - \mathbf{G})^{-1}\,\mathbf{Y}\,(\omega\mathbf{I} - \mathbf{G}^\top)^{-1}. \tag{23}$$

We use this result to prove the following Theorem (proof in Supplemental Material [6]):

Theorem 2. Let $\mathbf{G}$ be a convergent matrix, i.e., with a spectral radius less than 1, $\mathbf{Y}$ be a positive definite matrix, and $\mathbf{R}$ be a matrix with the following series expansion:

$$\begin{aligned}
\mathbf{R} &= (\mathbf{I} - \mathbf{G})^{-1}\mathbf{Y}(\mathbf{I} - \mathbf{G}^\top)^{-1} \\
&= \sum_{m=0}^{\infty}\sum_{\substack{j+k=m \\ j\geqslant 0,\, k\geqslant 0}} \mathbf{G}^j\,\mathbf{Y}\,(\mathbf{G}^\top)^k.
\end{aligned} \tag{24}$$

$\mathbf{S}_m := \sum_{\substack{j+k=m \\ j\geqslant 0,\, k\geqslant 0}} \mathbf{G}^j\,\mathbf{Y}\,(\mathbf{G}^\top)^k$ can be found by the following recursive algorithm:

$$\begin{aligned}
t_m &= \frac{2}{m}[\mathrm{Tr}(\mathbf{Y}^{-1}\mathbf{G}\mathbf{U}_{m-2}\mathbf{G}^\top) - \mathrm{Tr}(\mathbf{Y}^{-1}\mathbf{G}\mathbf{U}_{m-1})] \\
\mathbf{U}_m &= t_m\mathbf{Y} + \mathbf{G}\mathbf{U}_{m-1} + \mathbf{U}_{m-1}\mathbf{G}^\top - \mathbf{G}\mathbf{U}_{m-2}\mathbf{G}^\top \\
\mathbf{S}_m &= \mathbf{U}_m - \sum_{k=0}^{m-1} t_{m-k}\,\mathbf{S}_k,
\end{aligned} \tag{25}$$

starting with $m = 0$ until $m = 2n$ and the initial values $t_0 = 1$ and $\mathbf{U}_{-2} = \mathbf{U}_{-1} = \mathbf{0}$.

We will use this result in Sec. IV E to recursively find the terms of various orders in the power-series expansion of the integrated covariance matrix of a network of spiking neurons modeled by Hawkes processes [12].

IV. APPLICATIONS

We now apply the rational function solutions of Secs. II and III to compute the power spectra of a range of nonlinear models exhibiting fixed-point solutions and, where appropriate, we provide analytical closed-form expressions. We consider four models: (i) The stochastic Hindmarsh-Rose model simulating the subthreshold activity of a neuron subject to an input current [16,21]; (ii) a 4D Wilson-Cowan model simulating the activity of excitatory and inhibitory neuronal populations in the cortex [22,23]; (iii) the stochastic stabilized supralinear network (SSN) model [24,25], which is a neural circuit model for the sensory cortex approximating divisive normalization [26,27]; (iv) an evolutionary game-theoretic model which involves a population of agents playing a generalized version of the rock-paper-scissors game in n dimensions [28]. Additionally, we apply the recursive solution described in Theorem 2 to analyze the correlation structure of a network of spiking neurons, in random and ring networks, modeled by the Hawkes process [12].

A. Hindmarsh-Rose

Hindmarsh-Rose [16,21] is a phenomenological 3D neuron model that can be considered a simplification of the Hodgkin-Huxley equations [18] or a generalization of the FitzHugh-Nagumo model [13,15]. We consider a stochastic version of the model based on the implementation by Storace *et al.* [21]. The system of SDEs defining the model is given by

$$\begin{aligned}\frac{\mathrm{d}x}{\mathrm{d}t} &= y - x^3 + bx^2 + I - z + \sigma\eta_1\\ \frac{\mathrm{d}y}{\mathrm{d}t} &= 1 - 5x^2 - y\\ \frac{\mathrm{d}z}{\mathrm{d}t} &= \mu(s(x - x_{\mathrm{rest}}) - z).\end{aligned} \tag{26}$$

Here, x represents the membrane potential of the neuron, y is a recovery variable, and z is a slow adaptation variable. I represents the synaptic current input to the neuron; $\mu \ll 1$ controls the relative timescales between the fast subsystem (x, y) and the slow z variable; x_{rest} is the resting state of the membrane potential of the neuron; s governs adaptation; and b controls the transition of the activity to different dynamical states (quiescent, spiking, regular bursting, irregular bursting, and so on) [21]. We add Gaussian white noise, $\sigma\eta_1$, with standard deviation σ, to the membrane potential and choose the model parameters so that the system is in a quiescent (subthreshold) state with a single stable equilibrium, namely, $I = 5.5$, $b = 0.5$, $\mu = 0.01$, $x_{\mathrm{rest}} = -1.6$, $s = 4$, and $\sigma = 0.001$ [29].

Since the system is in a quiescent state, it exhibits a single fixed-point solution. Assuming that the deterministic steady state is given by the triplet (x_e, y_e, z_e), we can linearize the system about the fixed point and write Eq. (26) as the LTI system:

$$\begin{bmatrix}\dot{x}\\ \dot{y}\\ \dot{z}\end{bmatrix} = \begin{bmatrix}2bx_e - 3x_e^2 & 1 & -1\\ -10x_e & -1 & 0\\ \mu s & 0 & -\mu\end{bmatrix}\begin{bmatrix}x - x_e\\ y - y_e\\ z - z_e\end{bmatrix} + \begin{bmatrix}\sigma\eta_1\\ 0\\ 0\end{bmatrix}. \tag{27}$$

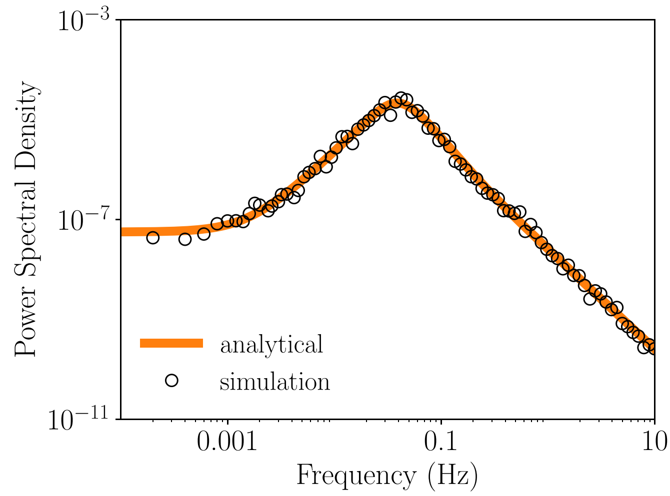

FIG. 3. Power spectrum of the Hindmarsh-Rose model. The power spectral density of the membrane potential x is calculated via simulation and our analytical (element-wise) solution. We use the following parameters to simulate the model: $I = 5.5$, $b = 0.5$, $\mu = 0.01$, $x_{\mathrm{rest}} = -1.6$, and $s = 4$. We consider the case of additive Gaussian white noise with standard deviation $\sigma = 0.001$.

To show how our element-wise solution leads to a closed-form expression for the power spectrum of the membrane potential, we use the general analytical solution for a 3D system given by Eq. (15):

$$\mathcal{S}_x(\omega) = \frac{Z(\omega)}{Q(\omega)} = \frac{p_0 + p_1\omega^2 + p_2\omega^4}{q_0 + q_1\omega^2 + q_2\omega^4 + q_3\omega^6}.$$

From the application of Eq. (12), we obtain the coefficients of the denominator, $Q(\omega)$, as

$$\begin{aligned}q_0 &= \mu^2(x_e(3x_e - 2b + 10) + s)^2\\ q_1 &= \mu^2((x_e(3x_e - 2b) + s)^2 - 20x_e + 1)\\ &\quad + x_e^2(3x_e - 2b + 10)^2 - 2\mu s + 20\mu s x_e\\ q_2 &= x_e(x_e(3x_e - 2b)^2 - 20) + \mu^2 - 2\mu s + 1\\ q_3 &= 1.\end{aligned} \tag{28}$$

Similarly, the coefficients of the numerator, $Z(\omega)$, can be found from Eq. (16): using the fact that $\sigma_1 = \sigma_2 = \sigma_3 = \sigma$, $l_1 = 1$, and $l_2 = l_3 = 0$, we obtain

$$\begin{aligned}p_0 &= \tfrac{1}{2}\sigma^2\big(\mathrm{Tr}^2\big(\mathbf{O}_{11}^2\big) - \mathrm{Tr}\big(\mathbf{O}_{11}^4\big)\big)\\ p_1 &= \sigma^2\mathrm{Tr}\big(\mathbf{O}_{11}^2\big)\\ p_2 &= \sigma^2.\end{aligned} \tag{29}$$

Now, plugging $\mathbf{O}_{11}$ given by

$$\mathbf{O}_{11} = \begin{bmatrix}-1 & 0\\ 0 & -\mu\end{bmatrix} \tag{30}$$

into the equation above yields the polynomial expansion of the numerator as

$$Z(\omega) = \mu^2\sigma^2 + (\mu^2 + 1)\sigma^2\omega^2 + \sigma^2\omega^4. \tag{31}$$

We simulate the 3D system and verify that the simulated spectrum matches with the analytical element-wise solution

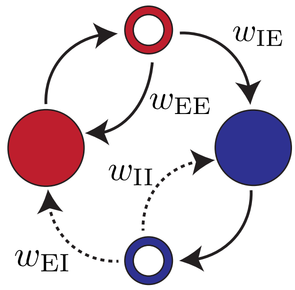

FIG. 4. Wilson-Cowan 4D model. The mean-field circuit consists of four variables modeling excitatory activity (solid red), inhibitory activity (solid blue), excitatory synaptic activity (hollow red), and inhibitory synaptic activity (hollow blue). The solid and dashed arrows indicate excitatory and inhibitory connections, respectively. w_{ij}, with $i, j \in \{\mathrm{E}, \mathrm{I}\}$, represents the weight associated with the connections from j to i.

we just derived, shown in Fig. 3. Furthermore, we calculate and plot the power spectral density for the membrane potential x, and the absolute cross-power spectral density and coherence between the fast variables x and y, using Welchs method [30] (simulation), the recursive and element-wise rational function solutions, and the "matrix solution" given by Eq. (3) (*n.b.*, this relies on a numerical inverse). We confirm that all the solutions match across the entire range of frequencies, see Supplemental Material, Fig. S3.

B. Wilson-Cowan model

The Wilson-Cowan model is a rate-based model that simulates the activity of excitatory (E) and inhibitory (I) populations of neurons and has been shown to exhibit gamma oscillations (30–120 Hz) for an appropriate choice of time constants [22]. Specifically, we consider a stochastic four-dimensional version of the model introduced by Keeley *et al.* [23], which includes dynamical variables describing the synaptic activation and the firing rate of the E and I populations, see Fig. 4 for an illustration. The stochastic dynamical system is defined by the following set of equations:

$$\begin{aligned}
\tau_{\mathrm{E}} \frac{\mathrm{d}r_{\mathrm{E}}}{\mathrm{d}t} &= -r_{\mathrm{E}} + f((I_{\mathrm{E}} + w_{\mathrm{EE}} s_{\mathrm{E}} - w_{\mathrm{EI}} s_{\mathrm{I}} - \theta_{\mathrm{E}})/\kappa_{\mathrm{E}}) + \sigma_r \eta_1 \\
\tau_{\mathrm{I}} \frac{\mathrm{d}r_{\mathrm{I}}}{\mathrm{d}t} &= -r_{\mathrm{I}} + f((I_{\mathrm{I}} + w_{\mathrm{IE}} s_{\mathrm{E}} - w_{\mathrm{II}} s_{\mathrm{I}} - \theta_{\mathrm{I}})/\kappa_{\mathrm{I}}) + \sigma_r \eta_2 \\
\tau_{s_{\mathrm{E}}} \frac{\mathrm{d}s_{\mathrm{E}}}{\mathrm{d}t} &= -s_{\mathrm{E}} + \gamma_{\mathrm{E}} r_{\mathrm{E}}(1 - s_{\mathrm{E}}) + s_{\mathrm{E}}^0 + \sigma_s \eta_3 \\
\tau_{s_{\mathrm{I}}} \frac{\mathrm{d}s_{\mathrm{I}}}{\mathrm{d}t} &= -s_{\mathrm{I}} + \gamma_{\mathrm{I}} r_{\mathrm{I}}(1 - s_{\mathrm{I}}) + s_{\mathrm{I}}^0 + \sigma_s \eta_4.
\end{aligned} \tag{32}$$

These equations describe the activity of E and I neurons at a population level, with r_{E} and r_{I} representing their firing rates, and s_{E} and s_{I} representing the corresponding synaptic activations. $w_{\alpha\beta}$, where α and $\beta \in \{\mathrm{E}, \mathrm{I}\}$ are the synaptic weights, and $f(x) = 1/(1 + e^{-x})$ is a sigmoid nonlinearity.

The input to the sigmoid is a weighted sum of the synaptic responses plus the external drives I_α, which are offset by θ_α and scaled by κ_α. The synaptic activity (s_α) for E and I populations evolves with time and depends on the firing rate of the corresponding population (r_α), scaled by γ_α, as well as on the corresponding background synaptic inputs s_α^0. The time constants controlling the rise/decay times are τ_α. The variables evolve stochastically on account of the uncorrelated Gaussian additive white noise, $\sigma\eta_i$, with standard deviations σ_r and σ_s, added to the firing rates and the synaptic activity, respectively.

We perform a simulation of the 4D system and generate power spectral density plots for the firing rate of the E population, r_{E}, the absolute cross-power spectral density between the firing rate of the E and I populations, and the coherence

$$K_{ij} = \frac{|\mathcal{S}_{ij}|^2}{|\mathcal{S}_{ii}||\mathcal{S}_{jj}|} \tag{33}$$

between the firing rates of the E and I populations using Welchs method [30] for simulation, the recursive and

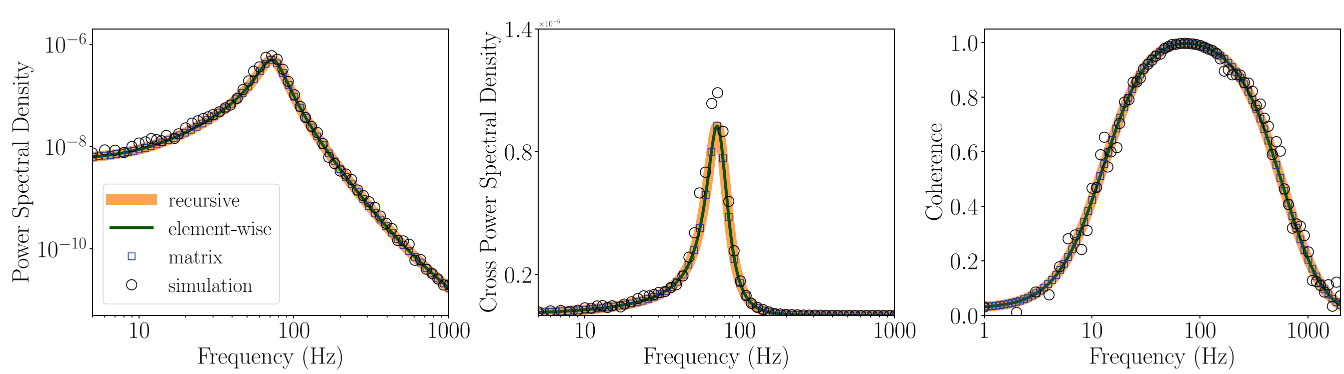

FIG. 5. Spectral density (auto and cross) and coherence for the Wilson-Cowan model. We plot the power spectral density (left), the absolute cross-power spectral density (middle), and the coherence (right) for a given stimulus, each calculated via simulation, the rational function solutions (recursive and element-wise), and the matrix solution [Eq. (3)]. The PSD is calculated for the firing rate of the excitatory population. The cross-PSD and coherence are calculated between the firing rates of the excitatory and inhibitory populations. We use the following parameters for simulations and analytical calculations. Time constants: $\tau_{\mathrm{E}} = 2\,\mathrm{ms}$, $\tau_{\mathrm{I}} = 8\,\mathrm{ms}$, $\tau_{s_{\mathrm{E}}} = 10\,\mathrm{ms}$, and $\tau_{s_{\mathrm{I}}} = 10\,\mathrm{ms}$. Strength of the weights: $w_{\mathrm{EE}} = 5$, $w_{\mathrm{EI}} = 5$, $w_{\mathrm{IE}} = 3.5$, and $w_{\mathrm{II}} = 3$. Offset of the input: $\theta_{\mathrm{E}} = 0.4$ and $\theta_{\mathrm{I}} = 0.4$. Scaling of the input: $\kappa_{\mathrm{E}} = 0.2$ and $\kappa_{\mathrm{I}} = 0.02$. Scaling of the population synaptic activity: $\gamma_{\mathrm{E}} = 1$ and $\gamma_{\mathrm{I}} = 2$. External inputs to the system: $I_{\mathrm{E}} = 1$, $I_{\mathrm{I}} = 0.5$, $s_{\mathrm{E}}^0 = 0.2$, and $s_{\mathrm{I}}^0 = 0.05$. We consider additive Gaussian white noise with standard deviations $\sigma_r = 0.001$, and $\sigma_s = 0.002$.

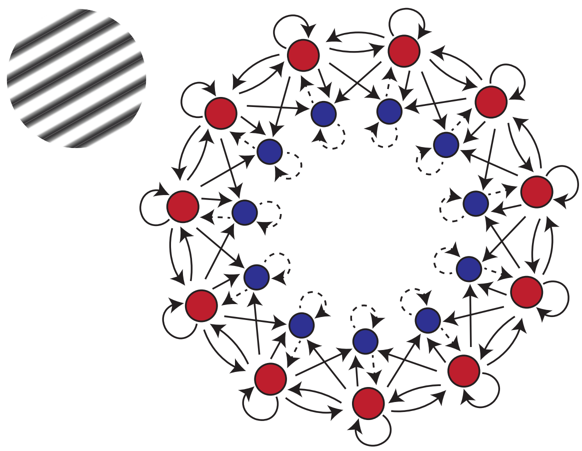

FIG. 6. SSN circuit. The circuit consists of 11 excitatory (red) and 11 inhibitory neurons (blue) and receives a sinusoidal grating input shown on the left. The arrows schematize the connections between the different neurons. E-E and I-E connections are excitatory (solid arrows) fully connected, whereas E-I and I-I connections are self-inhibitory (dashed arrows).

element-wise rational function solutions, and the matrix solution [Eq. (3)]. Our results demonstrate that all the solutions match across the entire range of frequencies, as confirmed in Fig. 5.

C. Stabilized supralinear network (SSN)

The stabilized supralinear network (SSN) [24,25] is a neural circuit model reproducing divisive normalization approximately [26,27] that has been used to simulate neuronal activity in the sensory cortex [24,25,31–33]. We implement an SSN for simulating the activity of the primary visual cortex (V1) as described in [24]. We consider a one-dimensional spatial input which is a sinusoidal grating of a fixed orientation and a given contrast (*n.b.*, the response of V1 neurons is tuned to specific positions, orientations, size, etc., of the visual stimulus [34]) and varies with Michelson contrast, $c = (I_{\max} - I_{\min})/(I_{\max} + I_{\min})$, where $I_{\min,\max}$ are the minimum and maximum luminance in the stimulus. The input evaluated at a set of discrete points $\mathbf{x}$ is taken to be proportional to the contrast, $\mathbf{h}(\mathbf{x}) \propto c$, and decays with distance from the origin (see Supplemental Material [6] for the precise functional form). We operate in a regime where the circuit exhibits a fixed-point solution with damped oscillations (for parameters see Fig. 7 and Supplemental Material [6]).

The dynamical equations for the firing rates of the excitatory neurons, $\mathbf{r}_{\mathrm{E}}(\mathbf{x})$, and the inhibitory neurons, $\mathbf{r}_{\mathrm{I}}(\mathbf{x})$, are given by

$$\tau_{\mathrm{E}} \frac{\mathrm{d}\mathbf{r}_{\mathrm{E}}(\mathbf{x})}{\mathrm{d}t} = -\mathbf{r}_{\mathrm{E}}(\mathbf{x}) + \mathbf{r}_{\mathrm{E}}^{ss}(\mathbf{x}) + \sigma\eta_{\mathrm{E}}(\mathbf{x}),$$
$$\tau_{\mathrm{I}} \frac{\mathrm{d}\mathbf{r}_{\mathrm{I}}(\mathbf{x})}{\mathrm{d}t} = -\mathbf{r}_{\mathrm{I}}(\mathbf{x}) + \mathbf{r}_{\mathrm{I}}^{ss}(\mathbf{x}) + \sigma\eta_{\mathrm{I}}(\mathbf{x}), \tag{34}$$

where τ_{E} and τ_{I} are the time constants of the excitatory and inhibitory neurons, $\sigma\eta_{\mathrm{E}}(\mathbf{x})$ and $\sigma\eta_{\mathrm{I}}(\mathbf{x})$ are zero-mean uncorrelated Gaussian noise vectors with standard deviation σ, and $\mathbf{r}_{\mathrm{E}}^{ss}$ and $\mathbf{r}_{\mathrm{I}}^{ss}$ are the steady-state responses of the excitatory and inhibitory neurons, given by the equations

$$\mathbf{r}_{\mathrm{E}}^{ss}(\mathbf{x}) = k([\mathbf{h}(\mathbf{x}) + \mathbf{W}_{\mathrm{EE}}\mathbf{r}_{\mathrm{E}}(\mathbf{x}) - \mathbf{W}_{\mathrm{EI}}\mathbf{r}_{\mathrm{I}}(\mathbf{x})]_{+})^{n},$$
$$\mathbf{r}_{\mathrm{I}}^{ss}(\mathbf{x}) = k([\mathbf{h}(\mathbf{x}) + \mathbf{W}_{\mathrm{IE}}\mathbf{r}_{\mathrm{E}}(\mathbf{x}) - \mathbf{W}_{\mathrm{II}}\mathbf{r}_{\mathrm{I}}(\mathbf{x})]_{+})^{n}. \tag{35}$$

Here, $[z]_{+} = \max(z, 0)$ denotes a ReLU activation. In the SSN, the steady-state responses depend on a supralinear activation ($n = 2.2$ and $k = 0.01$) of the input to the neurons, which is a sum of the stimulus input and feedback from the neurons in the population. The strength of the connections between E-E (excitatory to excitatory) and I-E (inhibitory to excitatory) neurons are encoded in the weight matrices $\mathbf{W}_{\mathrm{EE}}$ and $\mathbf{W}_{\mathrm{IE}}$, which decay like Gaussians as a function of distance from the preferred stimulus. The E-I and I-I connections are not fully connected but self-inhibitory, with diagonal weight matrices $\mathbf{W}_{\mathrm{EI}}$ and $\mathbf{W}_{\mathrm{II}}$, respectively.

We simulate a 22-dimensional system, see Fig. 6 for an illustration. In Fig. 7 we show the power spectral density for

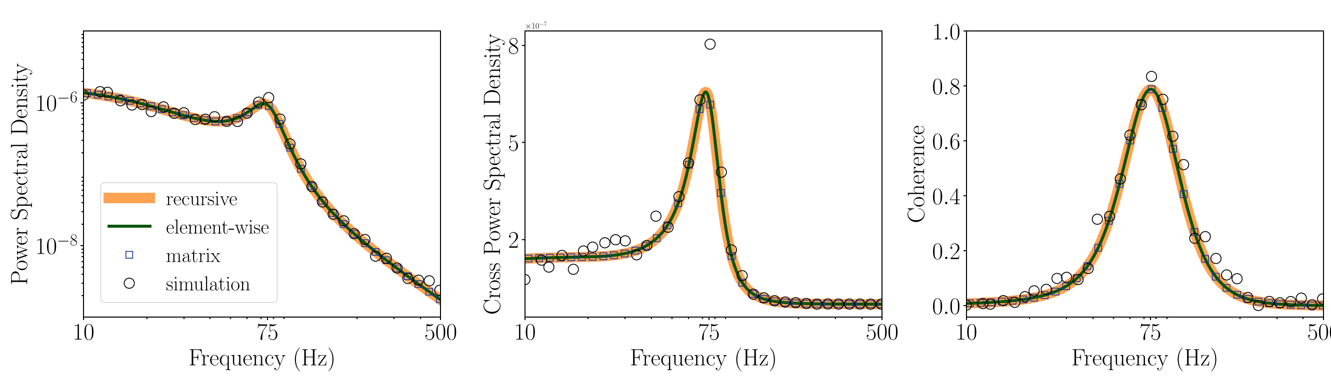

FIG. 7. Spectral density (auto and cross) and coherence for the SSN circuit. We plot the power spectral density (left), the absolute cross-power spectral density (middle), and the coherence (right) for a given stimulus each calculated via simulation, the rational function solutions (recursive and element-wise), and the matrix solution [Eq. (3)]. The PSD is calculated for the excitatory neuron with the highest preference for the stimulus (i.e., exhibiting maximum firing rate). The cross-PSD and coherence are calculated between the two excitatory neurons with the highest firing rates. We use the following parameters for simulating the model: contrast $c = 50$, stimulus length $l = 9$, $\Delta x = 3.0$, $\sigma_{\mathrm{RF}} = 0.125\Delta x$. Time constants of $\tau_{\mathrm{E}} = 6$ ms and $\tau_{\mathrm{I}} = 4$ ms. Supralinear activation parameters $n = 2.2$ and $k = 0.01$. See Supplemental Material [6] for the parameters associated with the weight matrices. We add zero-mean Gaussian noise to the SDEs describing the activity of the E and I neurons with standard deviation $\sigma = 0.01$.

the excitatory neuron with the highest preference for the stimulus (viz., that is maximally firing); the absolute cross-power spectral density and the coherence between the two excitatory neurons with the highest firing rates, each using Welchs method [30] (simulation); our recursive and element-wise rational function solutions; and the matrix solution [Eq. (3)]. We confirm that all the solutions match across the entire range of frequencies.

D. Rock-Paper-Scissors

The game of Rock-Paper-Scissors, where rock smashes scissors, scissors cut paper, and paper wraps rock, has been employed by evolutionary biologists to investigate the interactions between competing populations of species, where one species has an advantage over only one of its opponents. The game dynamics that describe the evolution of the populations following a particular strategy can be examined with the use of evolutionary game theory [28]. We explore the evolution of this dynamical system in accordance with a sociological model [35,36], where each population, following a unique strategy, seeks to minimize the difference between the average payoff of the population and the individual payoff.

Mathematically, we can represent the system as follows: Let $\mathbf{x} = [x_1, x_2, ..., x_n]$ be the n-dimensional system comprising the fractional populations corresponding to different strategies. The sociological model dictates that these fractional populations evolve according to a metric given by $\dot{x}_i \propto (f_{x_i} - \phi)$, where f_{x_i} is the individual payoff for choosing a strategy corresponding to the population x_i, and ϕ is the average payoff of the population given by $\phi = \sum_{i=1}^{n} x_i f_{x_i}$. It is important to note that the dynamical system is effectively $n-1$ dimensional due to the mass conservation equation $\sum_{i=1}^{n} x_i = 1$.

We consider a 31-dimensional ($n = 31$) version of the Rock-Paper-Scissors game, consisting of 31 populations each following a unique strategy, described by the pay-off matrix, $\mathbf{P}$. For an n-dimensional version of the game, the payoff matrix (P_{ij}) can be summarized as

$$P_{ij} = \begin{cases} (-1)^{i+j+1} & i > j \\ 0 & i = j \\ (-1)^{i+j} & i < j. \end{cases} \tag{36}$$

Here, 1 indicates a win against the opponent, -1 indicates a loss, and 0 indicates neither a win nor a loss (a draw). Therefore, the individual payoff for a given strategy is given in terms of $\mathbf{P}$ as $f_{x_i} = \sum_{j=1}^{n} P_{ij} x_j$.

In addition to the populations evolving according to the sociological strategy, we also consider the effects of global mutations and fluctuations in population. For the global mutations, we introduce a parameter μ such that each population mutates into every other population with constant rate μ, as illustrated in Fig. 8. This results in a stochastic dynamical system where the deterministic part evolves according to replicator-mutator dynamics [28,37]. Furthermore, we model the noise as multiplicative Gaussian white noise, $\sigma x_i \eta_i$, with standard deviation σ small enough that the population stays close to the fixed point. Thus, for the n-dimensional system, we can represent the set of differential equations for all $i \leqslant n$

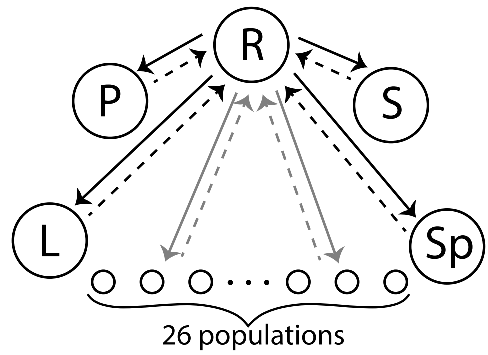

FIG. 8. 31-D Rock-Paper-Scissors model. Circles represent the different strategies ($n = 31$) in the evolutionary game-theoretic model. Shown in the figure are 5 of the 31 strategies: Rock (R), paper (P), Scissors (S), Spock (Sp), and Lizard (L). We consider a model with global mutations, i.e., each population associated with a strategy mutates into every other population with the same rate μ. Depicted in the figure are mutations to (dashed arrows) and from (solid arrows) the Rock population.

as follows:

$$\frac{\mathrm{d}x_i}{\mathrm{d}t} = x_i(f_{x_i} - \phi) + \mu\left(-(n-1)x_i + \sum_{\substack{j=1\\ j\neq i}}^{n} x_j\right) + \sigma x_i \eta_i. \tag{37}$$

To ensure that mass conservation is followed, we define the system according to the replicator-mutator differential equation [Eq. (37)] for $i \leqslant n-1$ and compute the nth population from the constraint $\sum_{i=1}^{n} x_i = 1$. Recall that the individual payoff is $f_{x_i} = \sum_{i=1}^{n} P_{ij} x_j$, and the average payoff of the population is $\phi = \sum_{i=1}^{n} x_i f_{x_i} = 0$. The dynamical system has a fixed point at $x_i^{ss} = 1/n$ for all $i \leqslant n$. Additionally, the elements of the Jacobian, J_{ij}, for the dynamical system evaluated at the fixed point can be defined as a function of the mutation rate parameter μ,

$$J_{ij} = \begin{cases} \begin{cases} 0 & j \text{ is even} \\ (-1)^i \times 2/n & j \text{ is odd} \end{cases} & i > j \\ (-1)^i/n - \mu n & i = j \\ \begin{cases} (-1)^i \times 2/n & j \text{ is even} \\ 0 & j \text{ is odd} \end{cases} & i < j. \end{cases} \tag{38}$$

We simulate a 31D system with a fixed mutation parameter, $\mu = 0.0005$, and the scaling factor of the noise, $\sigma = 10^{-4}$, that is the same for all the populations. In Fig. 9 (Fig. S4 for the five-dimensional, 5D, version) we show the power spectral density for the Rock population (viz., the first strategy), the absolute cross-power spectral density and the coherence between the Rock and Paper populations (viz., the first and second strategy), each using Welchs method [30] (simulation), our recursive and element-wise rational function solutions, and the matrix solution [Eq. (3)]. Our solutions match across the entire range of frequencies, verifying their correctness. See the Supplemental Material [6] for the analysis of a 5D Rock-Paper-Scissors-Lizard-Spock version of the game, alongside the analytical solution for its auto-spectrum. For this system it is possible to leverage the analytical coefficients

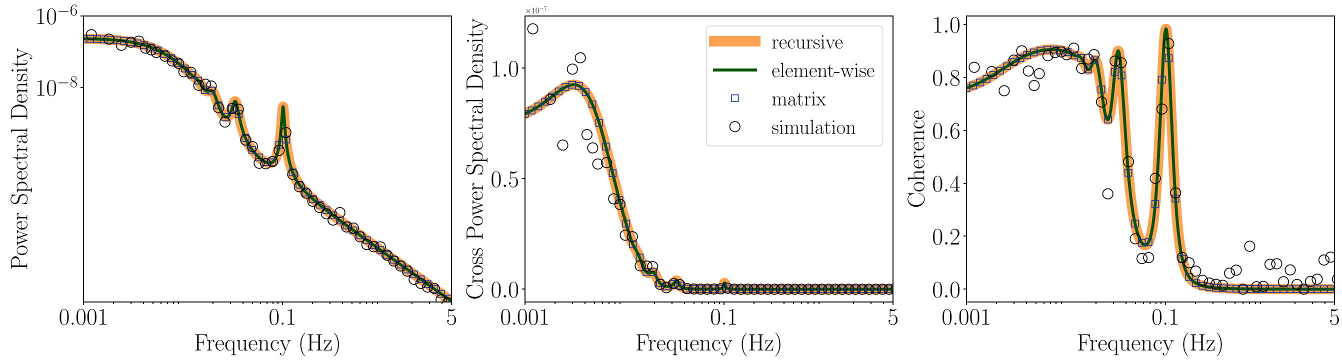

FIG. 9. Spectral density (auto and cross) and coherence using different methods for a 31-dimensional Rock-Paper-Scissors type model. We plot the power spectral density (left), the absolute cross-power spectral density (middle), and the coherence (right) for a fixed mutation parameter ($\mu = 0.0005$) each calculated via simulation, the rational function solutions, and the matrix solution. The PSD is calculated for the Rock population. The cross-PSD and coherence are calculated between the Rock and Paper populations. We consider the case of multiplicative noise, σx_j, added to each population, with standard deviation $\sigma = 10^{-4}$.

obtained by our rational function solution to derive analytical approximations that isolate the different features of the model (Fig. 10 and Supplemental Material [6]).

E. Hawkes model

Our final example shows how we can use Theorem 2 to find the connectivity-dependent correlation structure of spiking neurons connected in an arbitrary network. We consider the Hawkes model [12] describing recurrently connected linearly interacting spiking neurons, as in Ref. [38]. The network consists of linearly interacting point processes with recurrent connectivity given by the kernel matrix, $\mathbf{G}(t)$. The firing rates vector, $\mathbf{y}(t)$, evolves according to the Hawkes process, given by the following equation:

$$\mathbf{y}(t) = \mathbf{y}_0 + \int_{-\infty}^{t} \mathbf{G}(t-u)d\mathbf{N}(u), \tag{39}$$

where $\mathbf{N}(t)$ is the vector of point processes and $\mathbf{y}_0$ is a biasing vector encoding a constant external drive. Assuming a stationary state, the covariance matrix is defined by the following self-consistent equation:

$$\mathbf{R}(\tau) = \mathbf{G}(\tau)\mathbf{Y} + (\mathbf{G} * \mathbf{R})(\tau), \tag{40}$$

where $\mathbf{Y}$ is the diagonal matrix containing the entries of $\mathbf{y}_0$ on its diagonal and $*$ denotes convolution. The spectral density matrix of the Hawkes process is then given by [12]

$$\mathcal{S}(\omega) = (\mathbf{I} - \hat{\mathbf{G}}(\omega))^{-1}\,\mathbf{Y}\,(\mathbf{I} - \hat{\mathbf{G}}^{\top}(\omega))^{-1}, \tag{41}$$

where $\hat{\mathbf{G}}(\omega)$ is the Fourier transform of $\mathbf{G}(\tau)$. Then, the integrated covariance matrix $\mathbf{R} := \int_{-\infty}^{\infty} \mathbf{R}(\tau)\mathrm{d}\tau = \mathcal{S}(0)$ is given by

$$\mathbf{R} = (\mathbf{I} - \mathbf{G})^{-1}\mathbf{Y}(\mathbf{I} - \mathbf{G}^{\top})^{-1}, \tag{42}$$

where $\mathbf{G} := \int_{-\infty}^{\infty} \mathbf{G}(\tau)\mathrm{d}\tau = \hat{\mathbf{G}}(0)$.

We consider the problem of how the connectivity pattern influences the correlation structure in networks of spiking neurons, as studied in [38–40]. In particular, when the spectral radius of $\mathbf{G}$ is less than 1, we can expand the covariance matrix as the following infinite sum:

$$\mathbf{R} = \left(\sum_{j=0}^{\infty} \mathbf{G}^j\right)\mathbf{Y}\left(\sum_{k=0}^{\infty} (\mathbf{G}^{\top})^k\right) = \sum_{j,k=0}^{\infty} \mathbf{G}^j\,\mathbf{Y}(\mathbf{G}^{\top})^k = \sum_{m=0}^{\infty} \mathbf{S}_m, \tag{43}$$

where $\mathbf{S}_m := \sum_{\substack{j+k=m \\ j\geqslant 0,\, k\geqslant 0}} \mathbf{G}^j\,\mathbf{Y}\,(\mathbf{G}^{\top})^k$ accounts for the contributions of *paths* of order (length) m to the integrated covariance matrix. Note that for the (a, b)th entry of $\mathbf{G}^j\,\mathbf{Y}(\mathbf{G}^{\top})^k$, $\mathbf{G}^j$ represents the sum over all paths towards a from driving nodes c that are distance j from a, while $(\mathbf{G}^{\top})^k$ encodes the sum over all paths towards b from nodes c that are distance k from b. Then the total length of the paths between a and b through driving nodes c is $m = j + k$ [see Fig. 11(a) for an example].

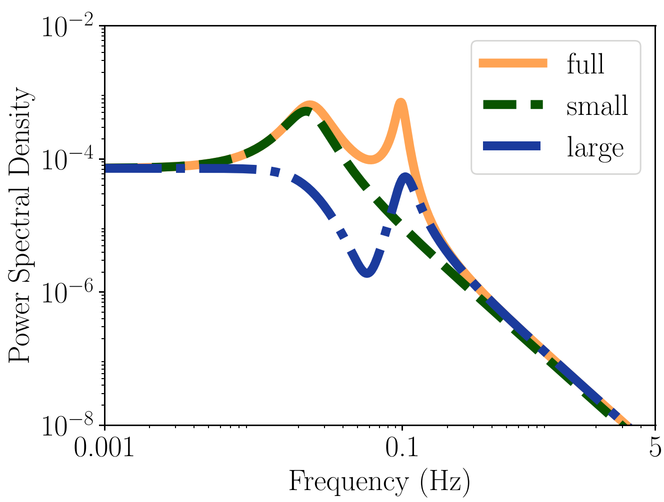

FIG. 10. Rational function solution for the spectral density in the Rock-Paper-Scissors-Lizard-Spock ($n = 5$) model. We plot the full rational function for the power spectral density of the "paper" population, and its analytical approximations isolating the low-frequency peak, $\mathcal{S}^{22}_{\text{small}}(\omega) = (p_0 + p_1\omega^2)/(q_0 + q_1\omega^2 + q_2\omega^4)$ and the high-frequency peak, $\mathcal{S}^{22}_{\text{large}}(\omega) = (p_0 + p_2\omega^4 + p_3\omega^6)/(q_0 + q_2\omega^4 + q_3\omega^6 + q_4\omega^8)$.

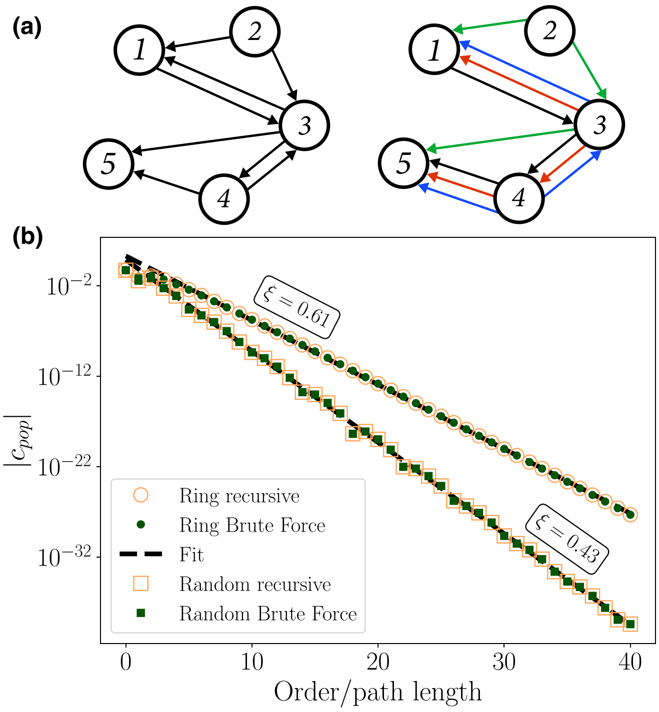

FIG. 11. Population covariance of spiking neural networks. (a) (Left) Directed graph representing the connectivity structure of a spiking network model. (Right) Third-order paths contributing to the ($a = 1, b = 5$) entry of $\mathbf{S}_3$ in the integrated covariance, Eq. (43). $c = 2, 3, 4$ are the intermediary nodes in the graph. Colored arrows represent the path between nodes $a = 1$ and $b = 5$ via (green) $c = 2$ and (red) $c = 3$ due to the term $\mathbf{G}\,\mathbf{Y}(\mathbf{G}^\top)^2$; (blue) via $c = 4$ due to the term $\mathbf{G}^2\,\mathbf{Y}(\mathbf{G}^\top)$; (black) direct path between nodes $a = 1$ and $b = 5$ due to the term $\mathbf{Y}(\mathbf{G}^\top)^3$. (b) Absolute average pairwise population covariance, $|c_{\mathrm{pop}}|$, as a function of path length m, found by calculating the mean of the matrix elements $\mathbf{S}_m$ in Eq. (43), for a directed cycle graph (circles), and a directed random graph (squares). The contributions $\mathbf{S}_m$ are computed by the recursive algorithm in Theorem 2 and by a brute force approach. The Hawkes models are defined by the following parameters: $N_E = 16$ (#E neurons), $N_I = 4$ (#I neurons), $g_E = 0.015$, $g_I = -0.075$. For the model on a random graph, the probability of drawing a directed edge between any two nodes (i, j) is 0.45.

Therefore, this quantity provides a way of quantifying how graph connectivity influences correlations in a network of spiking neurons modeled as a Hawkes process.

We demonstrate how the recursive algorithm in Theorem 2 allows us to compute $\mathbf{S}_m$ in $\mathcal{O}(n^4)$ compared to $\mathcal{O}(n^5)$ by a brute force solution. We consider two different types of networks, both described in detail in [38]. The first network has neurons (both E and I) in a ring structure with only connections between nearest neighbors allowed (i.e., in a bidirectional directed cycle graph). The second is a randomly connected network of E and I neurons (i.e., a random directed graph). The total number of neurons is 20, with 16 E and 8 I neurons, each receiving a constant input of 10 Hz, i.e., $y_0 = 10$ Hz. The kernels in matrix $\mathbf{G}(\tau)$ are exponentially decaying with a time constant of 10 ms and an amplitude of 1.5 Hz/−7.5 Hz for E/I spikes. This corresponds to the entries of the matrix $\mathbf{G}$ being 0.015 for E presynaptic neurons and −0.075 for I presynaptic neurons. For the randomly connected network, the oriented edge between neurons i and j is added with a probability 0.45, chosen so that the total number of connections for the ring model and the random model are equal.

Figure 11 shows the absolute average pairwise population covariance, $|c_{\mathrm{pop}}|$, as a function of path length m, found by calculating the mean of the matrix elements of $\mathbf{S}_m$, and confirms that the recursive solution (Theorem 2) matches the brute force solution. Moreover, since $|c_{\mathrm{pop}}|$ decays exponentially as a function of the order m, we estimate the typical order/path (correlation) length (ξ) by assuming the relation $|c_{\mathrm{pop}}| \propto e^{-m/\xi}$. Clearly, the network topology influences the characteristic path length, so that $\xi_{\mathrm{ring}} > \xi_{\mathrm{random}}$, despite both networks having the same number of connections.

V. DISCUSSION

In this work we presented two approaches for computing explicitly the rational function solution of the power spectral density matrix for stochastic linear time-invariant systems driven by Gaussian white noise. In one approach we derived element-wise solutions (valid for arbitrary n-dimensional LTI systems) for the rational function coefficients of any given entry of the PSD matrix, computable in roughly $\mathcal{O}(n^4 \log n)$ operations. Each coefficient is expressed in terms of Bell polynomials [19] evaluated on submatrices of the Jacobian, defined according to the algorithm summarized in Fig. 2. Our element-wise solution is particularly useful to gain insights into the dependence of the PSD on the model's functional form and its parameters, especially when the model is fairly low dimensional. Therefore, we provide explicit solutions for the auto-spectra of a general $n =$ 2-, 3-, and 4-dimensional system driven by uncorrelated Gaussian noise increments. A similar, albeit longer, symbolic expression can be obtained for any dimensional system and noise correlation structure via our software package (or working through the general solution in the Supplemental Material [6]), see Sec. V. We also showed that the polynomial matrix coefficients in the numerator and the polynomial coefficients in the denominator can be obtained recursively by means of a Faddeev-Leverrier–type algorithm in $\mathcal{O}(n^4)$ operations, see Theorem 1 [41]. Note that since we perform our numerical calculations with arbitrary precision our implementation scales $\mathcal{O}(n^5)$, see Supplemental Material [6]. Since the algorithm involves simple matrix multiplication and trace operations, it should be possible to further optimize it to achieve better time complexity. Crucially, both our solutions are free of matrix inverses, in addition to being more revealing than the simpler matrix solution given by Eq. (3).

Finally, we applied our approaches for the derivation of analytical (i.e., closed form) PSD of stochastic nonlinear dynamical models of neural systems, namely, FitzHugh-Nagumo ($n = 2$), Hindmarsh-Rose ($n = 3$), Wilson-Cowan ($n = 4$), and the stabilized supralinear network ($n = 22$), as well as of an evolutionary game-theoretic model with mutations ($n = 5, 31$).

To showcase the power of the recursive approach and its broad applicability, we used it to find a recursive solution for an auxiliary spectral matrix of similar form, Appendix B. This enabled us to derive a recursive algorithm (Theorem 2) for the terms of varying order in an expansion of the integrated covariance matrix for a network of linearly interacting spiking neurons modeled by Hawkes processes. The recursive nature of the solution not only leads to a faster algorithm [$\mathcal{O}(n^4)$ vs the $\mathcal{O}(n^5)$ of the brute force approach] but also provides deeper insights into the structure of the covariance matrix.

Since ω appears in different powers in both the numerator and denominator of the rational function of the power spectral density, we can neglect certain terms when they are small within the relevant range of ω. For example, in Fig. 9 we demonstrated how setting these small terms to zero in specific frequency regimes, both small and large, enables us to isolate the two peaks observed in the spectra of the paper population within the 5D Rock-Paper-Scissor-Lizard-Spock model. The analytical tractability of these solutions may enable us to rule out certain models, identify simpler ones (e.g., by providing insight into how model parameters contribute to spectral features), or to establish constraints on model parameters that ensure the presence of a peak in the spectra within a specified frequency range. This direction will be explored in future work.

Overall, our solutions should find broad applicability in the analysis of the dynamics of stochastic biological systems exhibiting fixed-point solutions, as well as in the broader context of dynamical systems and control theory.

VI. CODE AVAILABILITY

See Ref. [42] for the code for the general solutions of the auto- and cross-spectrum along with descriptions of the various dynamical systems (including the Hawkes model) considered in the manuscript.

ACKNOWLEDGMENTS

The authors are deeply grateful to David Heeger for many insightful discussions that motivated this work. The authors also acknowledge valuable discussions with Mathias Casiulis, Ruben Coen-Cagli, Lyndon Duong, and Flaviano Morone. This work was supported by the National Institute of Health under Award No. R01EY035242. S.M. acknowledges the Simons Center for Computational Physical Chemistry for financial support. This work was supported in part through the NYU IT High Performance Computing resources, services, and staff expertise.

APPENDIX A: RATIONAL FUNCTION DECOMPOSITION OF THE PSD

The power spectral density of the LTI SDE described in Eq. (2) can alternatively be written as the inverse of the Hermitian positive definite matrix (see Supplemental Material [6]), assuming that $\mathbf{C} \equiv \mathbf{L}\,\mathbf{D}\,\mathbf{L}^\top$ is positive definite:

$$\mathcal{S}(\omega) = [\mathbf{J}^\top\mathbf{C}^{-1}\mathbf{J} + \omega^2\mathbf{C}^{-1} + i\omega(\mathbf{J}^\top\mathbf{C}^{-1} - \mathbf{C}^{-1}\mathbf{J})]^{-1}. \tag{A1}$$

This enables us to efficiently compute the matrix inverse by Cholesky decomposition. We can recast $\mathcal{S}(\omega)$ as a rational function, and upon expanding Eq. (3) in terms of the adjugate and determinant matrices, we find

$$\begin{aligned}\mathcal{S}(\omega) &= (i\omega\mathbf{I} + \mathbf{J})^{-1}\,\mathbf{C}\,(-i\omega\mathbf{I} + \mathbf{J})^{-\top}\\ &= \frac{\mathrm{adj}(\mathbf{J} + i\omega\mathbf{I})\,\mathbf{C}\,\mathrm{adj}^\top(\mathbf{J} - i\omega\mathbf{I})}{\det(\mathbf{J} + i\omega\mathbf{I})\det(\mathbf{J} - i\omega\mathbf{I})}\\ &= \frac{\mathbf{Z}(\omega)}{Q(\omega)}.\end{aligned} \tag{A2}$$

Here, $\mathbf{Z}(\omega)$ is a complex polynomial matrix representing the numerator of the solution, and $Q(\omega)$ is an even-powered polynomial of degree $2n$ representing the denominator of the solution. When we express the adjugate of the matrices in terms of the corresponding cofactor matrices, it is apparent that $\mathbf{Z}(\omega)$ contains complex polynomials of degree $2n-2$, with even powers of ω being real and odd powers of ω being imaginary.

APPENDIX B: RECURSIVE ALGORITHM FOR AUXILIARY SPECTRAL MATRIX

Theorem 3. Let $\mathbf{G}$ be a real square matrix, $\mathbf{Y}$ be a positive definite matrix, and $\mathcal{T}(\omega)$ be defined as follows:

$$\begin{aligned}\mathcal{T}(\omega) &= (\omega\mathbf{I} - \mathbf{G})^{-1}\,\mathbf{Y}\,(\omega\mathbf{I} - \mathbf{G}^\top)^{-1}\\ &= \frac{\sum_{\alpha=0}^{2n-2}\mathbf{P}_\alpha\omega^\alpha}{\sum_{\alpha=0}^{2n}q_\alpha\omega^\alpha}.\end{aligned} \tag{B1}$$

The numerator's matrix coefficients are given by the recursive equations,

$$\mathbf{P}_{\alpha-1} = q_{\alpha+1}\mathbf{Y} + \mathbf{G}\mathbf{P}_\alpha + \mathbf{P}_\alpha\mathbf{G}^\top - \mathbf{G}\mathbf{P}_{\alpha+1}\mathbf{G}^\top, \tag{B2}$$

for $\alpha \in \{1, \ldots, 2n-1\}$, starting from $\alpha = 2n-1$ with $\mathbf{P}_{2n} = \mathbf{P}_{2n-1} = \mathbf{0}$. The scalar coefficients of the denominator can be recursively calculated using

$$q_\alpha = \frac{2}{2n-\alpha}[\mathrm{Tr}(\mathbf{Y}^{-1}\mathbf{G}\mathbf{P}_\alpha\mathbf{G}^\top) - \mathrm{Tr}(\mathbf{Y}^{-1}\mathbf{G}\mathbf{P}_{\alpha-1})] \tag{B3}$$

for $\alpha \in \{1, \ldots, 2n-1\}$, and $q_{2n} = 1$.

[1] P. Mondrian, Broadway Boogie Woogie, 1943.

[2] A. Einstein, Über die von der molekularkinetischen theorie der wärme geforderte bewegung von in ruhenden flüssigkeiten suspendierten teilchen, Ann. Phys. **322**, 549 (1905).

[3] P. Langevin, On the theory of Brownian motion, CR Acad. Sci. Paris **146**, 530 (1908).

[4] S. Särkkä and A. Solin, *Applied Stochastic Differential Equations* (Cambridge University Press, 2019), Vol. 10.

[5] C. W. Gardiner *et al.*, *Handbook of Stochastic Methods* (Springer, Berlin, 1985), Vol. 3.

[6] See Supplemental Material at http://link.aps.org/supplemental/10.1103/PhysRevResearch.6.043179 for the proof of recursive

solutions (spectrum and integrated covariance matrix) and a detailed description of the element-wise solution. Additional information and plots related to the various models can also be found here.

[7] T. Kailath, A view of three decades of linear filtering theory, IEEE Trans. Inf. Theory **20**, 146 (1974).

[8] A. H. Sayed and T. Kailath, A survey of spectral factorization methods, Numer. Linear Algebra Appl. **8**, 467 (2001).

[9] S.-H. Hou, Classroom note: A simple proof of the Leverrier–Faddeev characteristic polynomial algorithm, SIAM Rev. **40**, 706 (1998).

[10] D. K. Faddeev, V. N. Faddeeva, and R. C. Williams, *Computational Methods of Linear Algebra* (W. H. Freeman Company, 1963).

[11] D. S. Bernstein, *Matrix Mathematics Theory, Facts, and Formulas*, 2nd ed. (Princeton University Press, Princeton, 2009), p. 266.

[12] A. G. Hawkes, Point spectra of some mutually exciting point processes, J. R. Stat. Soc. B **33**, 438 (1971).

[13] R. FitzHugh, Impulses and physiological states in theoretical models of nerve membrane, Biophys. J. **1**, 445 (1961).

[14] J. Nagumo, S. Arimoto, and S. Yoshizawa, An active pulse transmission line simulating nerve axon, Proc. IRE **50**, 2061 (1962).

[15] M. E. Yamakou, T. D. Tran, L. H. Duc, and J. Jost, The stochastic FitzHugh–Nagumo neuron model in the excitable regime embeds a leaky integrate-and-fire model, J. Math. Biol. **79**, 509 (2019).

[16] J. L. Hindmarsh and R. Rose, A model of neuronal bursting using three coupled first order differential equations, Proc. R. Soc. London Ser. B **221**, 87 (1984).

[17] Note that Eq. (7) readily leads us to the correlation function $R(\tau) = \mathcal{F}^{-1}[S(\omega)] = \frac{\tau_r}{2}\sigma^2 e^{-|\tau|/\tau_r}$.

[18] A. L. Hodgkin and A. F. Huxley, A quantitative description of membrane current and its application to conduction and excitation in nerve, J. Phys. **117**, 500 (1952).

[19] E. T. Bell, Exponential polynomials, Ann. Math. **35**, 258 (1934).

[20] S. Barnett, Leverrier's algorithm: A new proof and extensions, SIAM J. Matrix Anal. Appl. **10**, 551 (1989).

[21] M. Storace, D. Linaro, and E. de Lange, The Hindmarsh–Rose neuron model: Bifurcation analysis and piecewise-linear approximations, Chaos **18**, 033128 (2008).

[22] H. R. Wilson and J. D. Cowan, Excitatory and inhibitory interactions in localized populations of model neurons, Biophys. J. **12**, 1 (1972).

[23] S. Keeley, Á. Byrne, A. Fenton, and J. Rinzel, Firing rate models for gamma oscillations, J. Neurophysiol. **121**, 2181 (2019).

[24] D. B. Rubin, S. D. Van Hooser, and K. D. Miller, The stabilized supralinear network: A unifying circuit motif underlying multi-input integration in sensory cortex, Neuron **85**, 402 (2015).

[25] Y. Ahmadian, D. B. Rubin, and K. D. Miller, Analysis of the stabilized supralinear network, Neural Comput. **25**, 1994 (2013).

[26] D. J. Heeger, Normalization of cell responses in cat striate cortex, Visual Neurosci. **9**, 181 (1992).

[27] M. Carandini and D. J. Heeger, Normalization as a canonical neural computation, Nat. Rev. Neurosci. **13**, 51 (2012).

[28] D. F. P. Toupo and S. H. Strogatz, Nonlinear dynamics of the rock-paper-scissors game with mutations, Phys. Rev. E **91**, 052907 (2015).

[29] We choose parameters in the pale cyan region of the bifurcation diagram in Fig. 1 of Ref. [21].

[30] P. Welch, The use of fast Fourier transform for the estimation of power spectra: A method based on time averaging over short, modified periodograms, IEEE Trans. Audio Electroacoust. **15**, 70 (1967).

[31] G. Hennequin, Y. Ahmadian, D. B. Rubin, M. Lengyel, and K. D. Miller, The dynamical regime of sensory cortex: Stable dynamics around a single stimulus-tuned attractor account for patterns of noise variability, Neuron **98**, 846 (2018).

[32] N. Kraynyukova and T. Tchumatchenko, Stabilized supralinear network can give rise to bistable, oscillatory, and persistent activity, Proc. Natl. Acad. Sci. USA **115**, 3464 (2018).

[33] C. J. Holt, K. D. Miller, and Y. Ahmadian, The stabilized supralinear network accounts for the contrast dependence of visual cortical gamma oscillations, PLoS Comput. Biol. **20**, e1012190 (2024).

[34] E. R. Kandel, J. H. Schwartz, T. M. Jessell, S. Siegelbaum, A. J. Hudspeth, S. Mack *et al.*, *Principles of Neural Science* (McGraw-Hill, New York, 2000), Vol. 4.

[35] I. M. Bomze, Lotka-Volterra equation and replicator dynamics: A two-dimensional classification, Biol. Cybern. **48**, 201 (1983).

[36] J. Hofbauer and K. Sigmund, Evolutionary game dynamics, Bull. Am. Math. Soc. **40**, 479 (2003).

[37] M. Mobilia, Oscillatory dynamics in rock–paper–scissors games with mutations, J. Theor. Biol. **264**, 1 (2010).

[38] V. Pernice, B. Staude, S. Cardanobile, and S. Rotter, How structure determines correlations in neuronal networks, PLoS Comput. Biol. **7**, e1002059 (2011).

[39] S. Ostojic, N. Brunel, and V. Hakim, How connectivity, background activity, and synaptic properties shape the cross-correlation between spike trains, J. Neurosci. **29**, 10234 (2009).

[40] J. Trousdale, Y. Hu, E. Shea-Brown, and K. Josić, Impact of network structure and cellular response on spike time correlations, PLoS Comput. Biol. **8**, e1002408 (2012).

[41] Note that since we perform our numerical calculations with arbitrary precision our implementation scales $\mathcal{O}(n^5)$, see Supplemental Material [6].

[42] Github: https://github.com/martiniani-lab/spectre.